

## Article

# Selective and Efficient Olefin Epoxidation by Robust Magnetic Mo Nanocatalysts

Cristina I. Fernandes <sup>1</sup>, Pedro D. Vaz <sup>2,3</sup>  and Carla D. Nunes <sup>1,\*</sup> 

<sup>1</sup> Centro de Química Estrutural, Departamento de Química e Bioquímica, Faculdade de Ciências, Universidade de Lisboa, 1749-016 Lisboa, Portugal; cifernandes@ciencias.ulisboa.pt

<sup>2</sup> CICECO—Aveiro Institute of Materials, Department of Chemistry, University of Aveiro, 3810-193 Aveiro, Portugal; pedro.vaz@fundacaochampalimaud.pt

<sup>3</sup> Champalimaud Foundation, Champalimaud Centre for the Unknown, 1400-038 Lisbon, Portugal

\* Correspondence: cmnunes@ciencias.ulisboa.pt

**Abstract:** Iron oxide magnetic nanoparticles were synthesized with different sizes (11 and 30 nm). Subsequently they were shelled with a silica layer allowing grafting of an organic phosphine ligand that coordinated to the [MoI<sub>2</sub>(CO)<sub>3</sub>] organometallic core. The silica layer was prepared by the Stöber method using either mechanical (both 11 and 30 nm nanoparticles) or ultrasound (30 nm only) stirring. The latter nanoparticles once coated with silica were obtained with less aggregation, which was beneficial for the final material holding the organometallic moiety. The Mo loadings were found to be 0.20, 0.18, and 0.34 mmol<sub>Mo</sub>·g<sup>-1</sup> for **MNP<sub>30</sub>-Si-phos-Mo**, **MNP<sub>11</sub>-Si-phos-Mo**, and **MNP<sub>30</sub>-Si<sub>us</sub>-phos-Mo**, respectively, with the ligand-to-metal ratio reaching 4.6, 4.8, and 3.2, by the same order, confirming coordination of the Mo moieties to two **phos** ligands. Structural characterization obtained from powder X-ray diffraction (XRD), scanning electron microscopy (SEM)/ transmission electron microscopy (TEM) analysis, and Fourier-transform infrared (FTIR) spectroscopy data confirmed the successful synthesis of all nanomaterials. Olefin epoxidation of several substrates catalyzed by these organometallic nano-hybrid materials using *tert*-butyl hydroperoxide (tbhp) as oxidant, achieved very good results. Extensive testing of the catalysts showed that they are highly active, selective, recyclable, and efficient concerning oxidant consumption.

**Keywords:** catalysis; core-shell; epoxidation; magnetic nanoparticles; molybdenum; recyclability



**Citation:** Fernandes, C.I.; Vaz, P.D.; Nunes, C.D. Selective and Efficient Olefin Epoxidation by Robust Magnetic Mo Nanocatalysts. *Catalysts* **2021**, *11*, 380. <https://doi.org/10.3390/catal11030380>

Academic Editor: Leonarda Francesca Liotta

Received: 9 February 2021  
Accepted: 10 March 2021  
Published: 15 March 2021

**Publisher's Note:** MDPI stays neutral with regard to jurisdictional claims in published maps and institutional affiliations.



**Copyright:** © 2021 by the authors. Licensee MDPI, Basel, Switzerland. This article is an open access article distributed under the terms and conditions of the Creative Commons Attribution (CC BY) license (<https://creativecommons.org/licenses/by/4.0/>).

## 1. Introduction

The development of nanosized chemical systems has become in recent years the focus of many research teams around the globe. The motivation to downsize chemical systems down to the nanoscale led to a huge increase in the edge knowledge concerning mastering the chemistry behind these systems alongside their applications. However, bottom-up approaches have proved to be far more successful than the more classic top-down. The research arising from this topic yielded applications of nanoparticles in many fields, including sensing, energy, biomedicine, or catalysis, among others [1,2].

Within the universe of nanoparticles, magnetic iron oxide nanoparticles have been widely used in recent years in many different areas, such as, catalysis, magnetic separation, imaging, drug delivery, among others [3–7]. However, this type of nanoparticles presents a high trend to agglomeration or degradation once exposed to biological systems [8–10]. Therefore, magnetic nanoparticles coating offers an alternative to the above problems, highlighting the silica coating using the Stöber method [11].

Silica presents some advantages such as, non-toxic to the organism, easy to manufacture and stable in most chemical and biological systems. It has also a high concentration of active Si-OH groups on its surface that allows functionalization of magnetic nanoparticles with a variety of species [12].

However, protection of magnetic nanoparticles core with silica coating does not prevent its aggregation. To take full advantage of the magnetic capabilities of iron oxide nanoparticles, a method of coating the nanoparticles has been described in the literature that combines mechanical stirring with ultrasonication resulting in the formation of more dispersed magnetic nanoparticles and higher magnetization [13].

Olefin epoxidation is considered one of the most relevant reactions for the industry due to the importance of epoxides in the production of various products such as resins, paints, and surfactants, and are also important intermediates in the production of pharmaceutical products, such as styrene oxide [14–16].

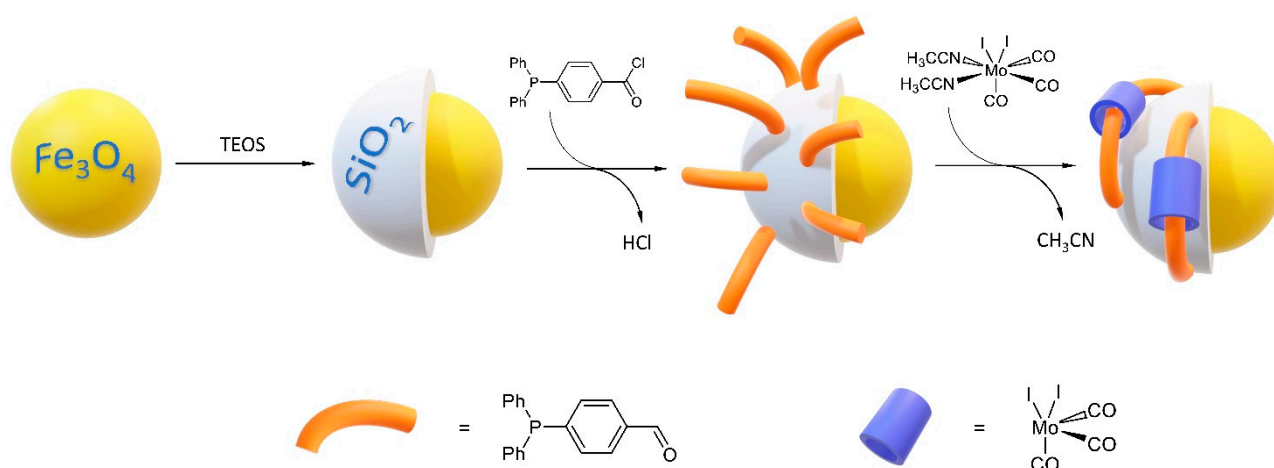
Progressing our research on catalytic olefin epoxidation [17–19], we present in this work the synthesis and catalytic assessment of a series of catalysts based on a Mo complex tethered to the surface of silica-shelled magnetic iron oxide nanoparticles with different dimensions. After preparation of the magnetic iron oxide cores, these nanoparticles were subsequently coated with silica, using two different methods, for stabilization. In this step, we explored the synthesis method by using regular mechanical stirring or ultrasound energy. The silica layer allowed grafting of an organic phosphine ligand. The latter coordinated to a Mo organometallic complex. The resulting nanomaterials were tested in the catalytic epoxidation of olefins. These nanocatalysts were quite active for that transformation with the advantage of being effortlessly separated from the reaction slurry with a magnet. This is critical to separate the catalyst and recycle it without jeopardizing product recovery, usually a laborious step in homogeneous systems.

## 2. Results and Discussion

### 2.1. Synthesis and Characterization of Magnetic Nanoparticles

MNP<sub>30</sub> and MNP<sub>11</sub> magnetic iron oxide nanoparticles with 30 and 11 nm diameter, respectively, were prepared by co-precipitation starting from a mixture of iron (II) and iron (III) chloride salts with ammonia, by a procedure described in the literature [20,21]. Subsequently the particles were coated with a dense silica layer, adopting the Stöber method, using tetraethyl orthosilicate (TEOS) and ammonia as silica source and hydrolyzing agent generating MNP<sub>30</sub>-Si and MNP<sub>11</sub>-Si materials. The silica coated system stabilizes the iron oxide core while providing the proper binding sites (Si-OH) for grafting the molecular catalysts. The MNP<sub>30</sub>-Si<sub>us</sub> magnetic nanoparticle equivalents also with 30 nm diameter were prepared using the same Stöber method as described above but using ultrasonication instead of mechanical stirring. The particles coated by this procedure were obtained in a more dispersed fashion and without too much aggregation [22,23]. Afterwards, the surface silanol groups (Si-OH units) of all the prepared materials were grafted with the phosCl ligand to materials MNP<sub>30</sub>-Si, MNP<sub>11</sub>-Si and MNP<sub>30</sub>-Si<sub>us</sub>, yielding MNP<sub>30</sub>-Si-phos, MNP<sub>11</sub>-Si-phos, and MNP<sub>30</sub>-Si<sub>us</sub>-phos, respectively [24,25]. Reaction of MNP<sub>30</sub>-Si-phos, MNP<sub>11</sub>-Si-phos, and MNP<sub>30</sub>-Si<sub>us</sub>-phos with the [MoI<sub>2</sub>(CO)<sub>3</sub>(CH<sub>3</sub>CN)<sub>2</sub>] precursor complex, originated the MNP<sub>30</sub>-Si-phos-Mo, MNP<sub>11</sub>-Si-phos-Mo, and MNP<sub>30</sub>-Si<sub>us</sub>-phos-Mo materials by the same order. The synthetic pathway is sketched in Scheme 1.

According to elemental analysis the ligand loading in MNP<sub>30</sub>-Si-phos, MNP<sub>11</sub>-Si-phos, and MNP<sub>30</sub>-Si<sub>us</sub>-phos taking in account the P content in all materials was found to be 2.84%, 2.66%, and 3.38%, respectively. This corresponds to a loading of 0.92 mmol·g<sup>-1</sup>, 0.86 mmol·g<sup>-1</sup>, and 1.09 mmol·g<sup>-1</sup> of the ligand bound to the surface silanol groups of the nanoparticles.



**Scheme 1.** Preparation of Mo(II) organometallic complex tethered to magnetic iron oxide nanoparticles.

The metal content in the magnetic nanoparticles **MNP<sub>30</sub>-Si-phos-Mo**, **MNP<sub>11</sub>-Si-phos-Mo**, and **MNP<sub>30</sub>-Si<sub>us</sub>-phos-Mo** was determined experimentally to be 1.89, 1.75, and 3.26 wt-% Mo, respectively, corresponding to a loading of 0.20, 0.18, and 0.34 mmol<sub>Mo</sub>·g<sup>-1</sup>, respectively. Based on these values, the ligand-to-metal ratio reached 4.6, 4.8 and 3.2, by the same order, which was consistent with the rationalization of the Mo moieties coordinated to two **phos** ligands.

The phase and purity of the as-obtained samples were examined by powder XRD, which agree with the published data and make possible to verify that the materials have the magnetite structure [21]. The powder X-ray diffraction (XRD) patterns of **MNP<sub>11</sub>** (Figure S1) and **MNP<sub>30</sub>** (Figure 1) exhibited the typical diffraction peaks assigned to the structure of magnetite (Fe<sub>3</sub>O<sub>4</sub>), Figure 1. The diffraction peaks could be indexed to face-centered cubic structure of magnetite according to JCPDS card No. 75-1609. Six characteristic peaks at  $2\theta$  values of 30.2°, 35.6°, 43.3°, 57.2°, and 62.9°, were indexed to the (220), (311), (400), (511), and (440) planes of the Fe<sub>3</sub>O<sub>4</sub> nanoparticles, respectively. Deduced from Debye–Scherrer’s equation,  $v = (Kl)/(\beta \cos \theta_B)$ , where  $K$  is the shape factor (0.94 was used in the calculation assuming spherical particles),  $\lambda$  is the wavelength of the radiation (Cu K $\alpha$  = 1.54 Å) and  $\beta$  is the peak full width at half maximum in radian, and based on both the (311) and (400) diffraction peaks, the average size of the Fe<sub>3</sub>O<sub>4</sub> MNPs found using both diffraction peaks, was ca. 11 and 30 nm, for **MNP<sub>11</sub>** and **MNP<sub>30</sub>**, respectively after calculation with Scherrer’s equation. Figure 1 also displays the XRD powder pattern of **MNP<sub>30</sub>-Si<sub>us</sub>**, which exhibited the typical magnetite structure (Fe<sub>3</sub>O<sub>4</sub>) diffraction peaks almost unchanged from the counterpart sample **MNP<sub>30</sub>**. Subsequent reactions with the ligand and the Mo organometallic moiety, yielding **MNP<sub>30</sub>-Si<sub>us</sub>-phos** and **MNP<sub>30</sub>-Si<sub>us</sub>-phos-Mo** materials, did not change the structure of the magnetite core, as presented in Figure 1 [20]. For the same series of material based on the mechanical stirring synthesis protocol (**MNP<sub>11</sub>-Si** and **MNP<sub>30</sub>-Si**) similar XRD powder patterns were obtained as already observed for the other counterpart MNPs, as shown in Figure S1 [20].

As revealed by transmission electron microscopy (TEM), the magnetic iron oxide nanoparticles **MNP<sub>30</sub>** and **MNP<sub>11</sub>** (Figure 2a,b) showed relatively uniform magnetite particles with average diameters of ca. 30 nm and 11 nm, respectively, in good agreement with powder XRD data (discussion above). From the particle size distribution histograms (Figure S3), it was found that the particle dimensions were  $11 \pm 7$  nm and  $31 \pm 15$  nm for **MNP<sub>30</sub>** and **MNP<sub>11</sub>**, respectively. From the histograms it becomes clear that the different synthesis protocols will yield different size distributions. However, these results also showed that the smaller **MNP<sub>11</sub>** were produced by an adequate method where size control is more critical than for **MNP<sub>30</sub>**.

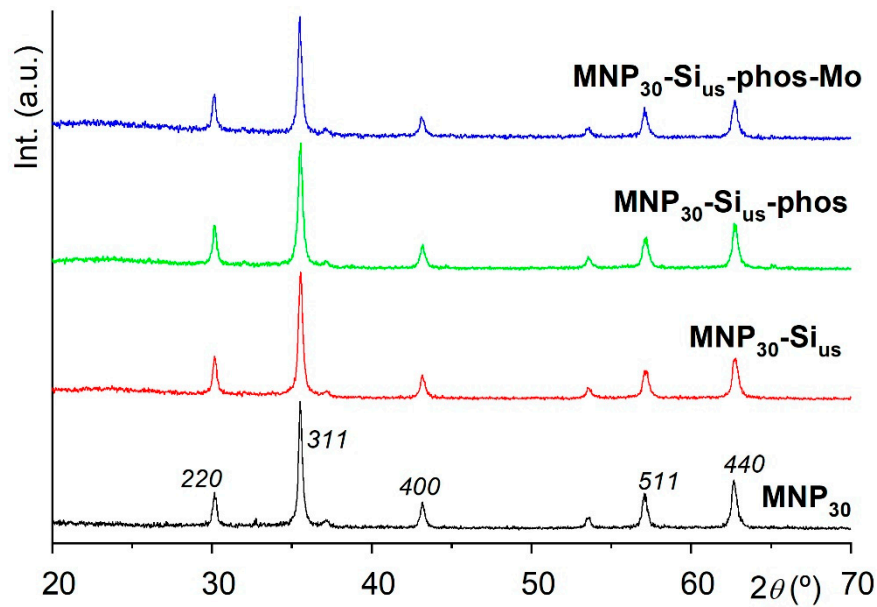


**Figure 1.** Powder XRD patterns of all materials prepared through the ultrasonication path starting from  $\text{MNP}_{30}$  (bottom) are shown. Labels show the most relevant magnetite ( $\text{Fe}_3\text{O}_4$ ) plans.

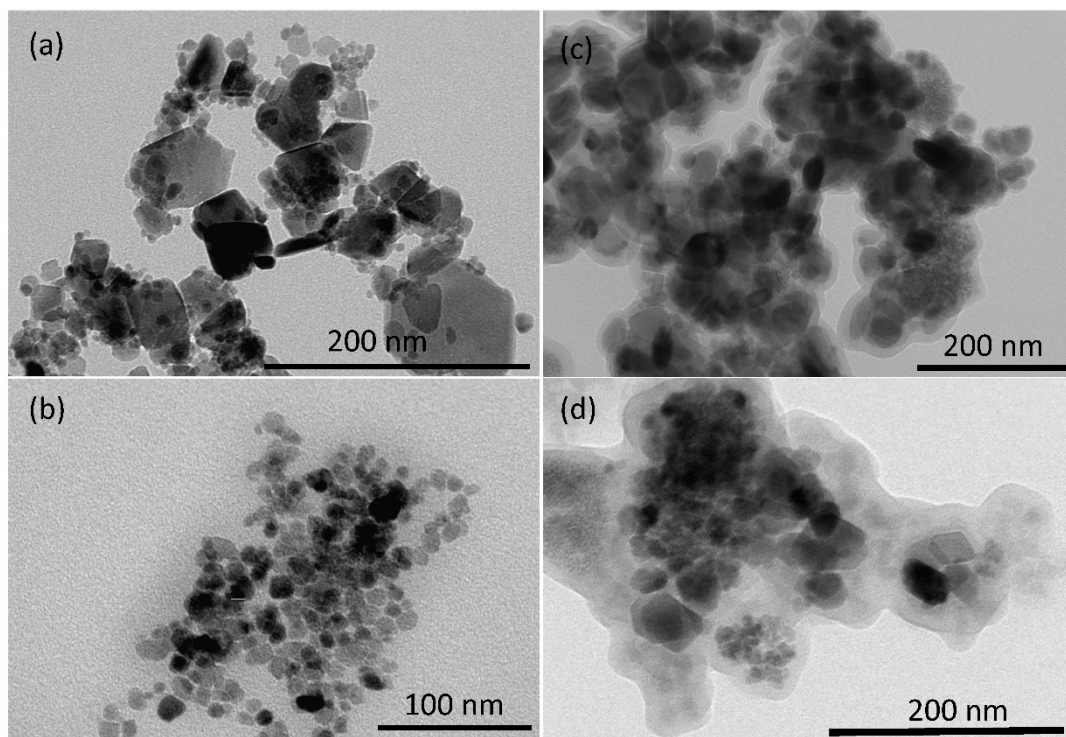


**Figure 2.** Transmission electron microscopy (TEM) images of  $\text{MNP}_{30}$  (a),  $\text{MNP}_{11}$  (b),  $\text{MNP}_{30}\text{-Si}$  (c) and  $\text{MNP}_{30}\text{-Si}_{\text{US}}$  (d) materials.

As seen in Figure 2c, the silica coated magnetic particles exhibited perfectly spherical shape with smooth surface and presented clear core-shell structure, although with some aggregation. The core-shell  $\text{MNP}_{30}\text{-Si}$  microspheres had a uniform silica coating and depth. The core-shell structure of the nanoparticles persisted undamaged throughout the derivatization reactions. On the other hand, the ultrasonicated core-shell magnetic iron oxide nanoparticles  $\text{MNP}_{30}\text{-Si}_{\text{US}}$  (Figure 2d) exhibited a uniform silica coating and thickness with almost no agglomeration than that evidenced by the  $\text{MNP}_{30}\text{-Si}$  (Figure 2c) material.

For comparison of the synthesis protocol outcome between mechanical and ultrasound stirring, scanning electron microscopy (SEM) evidenced some differences. SEM images show that  $\text{MNP}_{30}$  (Figure S2a) exhibited aggregated spherical particles with uneven external surfaces, and upon silica coating the resultant  $\text{MNP}_{30}\text{-Si}$  nanoparticles (Figure S2b) exhibited smooth and spongy surface showing the successful silica shelling of the magnetic nanoparticles. By comparison, analyzing the SEM image from the  $\text{MNP}_{30}\text{-Si}_{\text{us}}$  nanoparticles (Figure S2c) it was possible to observe that the particles were spherical, aggregated and they also had a smooth and spongy surface evidencing that the coating of the magnetic nanoparticles with silica was successful as well. However, Figure S2c also evidences that the SEM image shows more defined contours in the nanoparticles synthesized by this ultrasound route for the Stöber method as compared to those prepared via the traditional mechanical stirring (Figure S2b).

The Fourier-transform infrared FTIR spectra of all synthesized materials were also measured (Figure 3, only the ultrasound materials are shown). The  $\text{MNP}_{30}$  (and  $\text{MNP}_{11}$ , Figure S4) materials presented FTIR spectra that showed a band corresponding to the  $\nu\text{Fe-O}$  stretching at  $572\text{ cm}^{-1}$  and  $565\text{ cm}^{-1}$ , respectively, as evidenced in Figure 3.

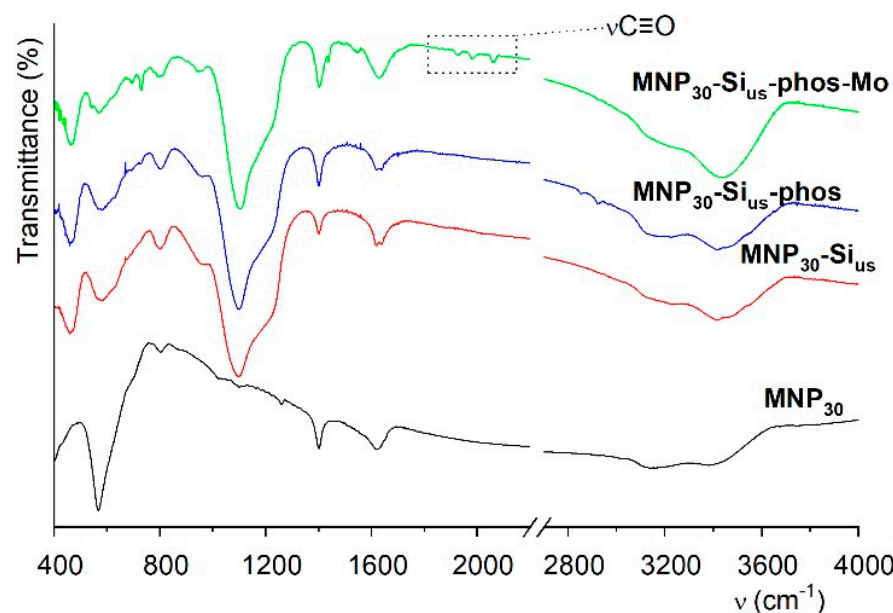


**Figure 3.** Fourier-transform infrared FTIR spectra of  $\text{MNP}_{30}$  derived materials by ultrasonication route. The dotted box highlights the  $\nu\text{C}\equiv\text{O}$  modes denoting presence of the  $[\text{Mo}_2(\text{CO})_3]$  moiety.

Moreover, the spectra also showed faint bands at  $2920\text{ cm}^{-1}$  and  $2852\text{ cm}^{-1}$  ( $\nu\text{C-H}$  modes) and at  $1618\text{ cm}^{-1}$  ( $\nu\text{C-O}$  mode) and  $1402\text{ cm}^{-1}$  ( $\nu\text{C=C}$  mode) arising from the oleic acid stabilizer. The  $\text{MNP}_{30}\text{-Si}_{\text{us}}$  material, obtained after silica coating, showed an additional intense broad band appearing at  $1092\text{ cm}^{-1}$  and  $1067\text{ cm}^{-1}$ , assigned to the  $\nu\text{Si-O}$  modes [26]. Upon ligand binding,  $\text{MNP}_{30}\text{-Si}_{\text{us}}\text{-phos}$  material showed additional bands at  $1709\text{ cm}^{-1}$  in the FTIR spectra, assigned to the  $\nu\text{C=O}$  stretching mode of the carbonyl group, and at  $3009\text{ cm}^{-1}$  due to the  $\nu\text{C-H}_{\text{arom}}$  stretching modes of the anchored **phos** ligand. A band at around  $1400\text{ cm}^{-1}$  was also observed, which was assigned to the  $\nu\text{C=C}_{\text{arom}}$  mode, confirming anchoring of the **phos** ligand at the surface of both materials (Figure 3).

Coordination of the organometallic  $[\text{Mo}_2(\text{CO})_3]$  fragment to the anchored **phos** ligand yielded the  $\text{MNP}_{30}\text{-Si}_{\text{us}}\text{-phos-Mo}$  material. In its FTIR spectrum, there were slight changes in the fingerprint region ( $1800\text{--}1200\text{ cm}^{-1}$ ), mostly evidenced by changes in the intensity rather than on the position of the bands. However, the solidest proof supporting the coordination and conservation of the  $[\text{Mo}_2(\text{CO})_3]$  moiety was given by the presence of the bands from the  $\nu\text{C}\equiv\text{O}$  modes, shifting from  $2072$ ,  $2016$  and  $1921\text{ cm}^{-1}$  in the precursor

complex [27], to 2062, 1982, and 1929  $\text{cm}^{-1}$  in **MNP<sub>30</sub>-Si<sub>us</sub>-phos-Mo** as shown in Figure 3. The position of the bands was in agreement with other systems from the literature [18]. Moreover, the lack of the  $\nu\text{C}\equiv\text{N}$  modes at ca. 2300  $\text{cm}^{-1}$  concomitantly with the strong shift of the  $\nu\text{C}\equiv\text{O}$  modes relatively to the precursor complex, confirmed that the  $[\text{MoI}_2(\text{CO})_3]$  moiety was coordinated to the **phos** ligand, which corroborates elemental analysis data. FTIR results obtained for the **MNP<sub>11</sub>** and **MNP<sub>30</sub>** set of materials were similar and are shown in Figure S3.

## 2.2. Catalytic Studies

The prepared **MNP<sub>30</sub>-Si-phos-Mo**, **MNP<sub>11</sub>-Si-phos-Mo**, and **MNP<sub>30</sub>-Si<sub>us</sub>-phos-Mo** materials were assessed as catalyst precursors for the epoxidation of olefins and allylic alcohols using two groups of substrates. Simple olefins, *cis*-cyclooctene and styrene, were the first group, while multifunctional olefins, *trans*-hex-2-en-1-ol and *R*-(+)-limonene were in the second group. *tert*-Butyl hydroperoxide (tbhp in decane) was used as oxidant in all reactions, and testing different solvents, namely, acetonitrile, toluene, and decane, at 353 K, 383 K, and 393 K, respectively.

Blank runs (without catalyst but with oxidizing agent) using *cis*-cyclooctene as substrate did not convert it to any oxidation product expressively yielding only ca. 3% cyclooctene oxide at 383 K in toluene.

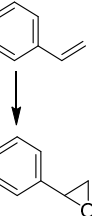
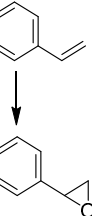
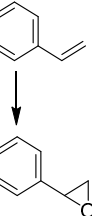
In the epoxidation of *cis*-cyclooctene all materials catalyzed selectively the oxidation of the substrate to the corresponding epoxide without formation of any by products (Table 1, entries 1–12). The catalysts showed to be very active in substrate conversion being obtained values in between 75% to 99%. The only exceptions were for the **MNP<sub>30</sub>-Si-phos-Mo** and **MNP<sub>30</sub>-Si<sub>us</sub>-phos-Mo** catalysts when the reactions were conducted using decane at 393 K originating only 53% and 52% conversion (Table 1, entries 4 and 12), respectively. With decane the temperature was raised out again, and the least enthusiastic results were obtained overall. A reason to explain this performance may be related with uncontrolled side-reactions that may occur including inefficient tbhp decomposition, which could lead to lower catalytic performance.

Styrene was converted very efficiently by all three catalysts with about 100% conversion for all the tested conditions (Table 1, entries 13–24). However, selectivity to the epoxide after 24 h of reaction was very low for the epoxidations in the presence of **MNP<sub>30</sub>-Si-phos-Mo** and **MNP<sub>11</sub>-Si-phos-Mo**, and **MNP<sub>30</sub>-Si<sub>us</sub>-phos-Mo** catalysts, meaning that the main product was benzaldehyde and not the expected epoxide. This occurred since styrene epoxide further reacted, through an oxidative cleavage mechanism [28], producing benzaldehyde, as described in the literature for analogous magnetic catalysts [20,21,29,30].

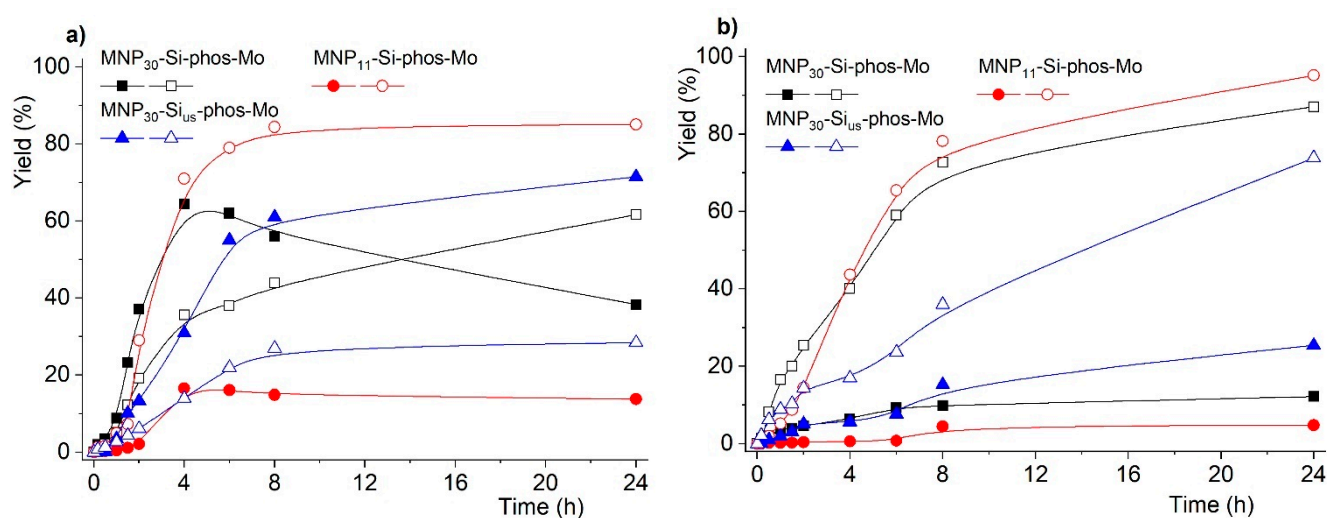
However, catalytic tests in the presence of the **MNP<sub>30</sub>-Si<sub>us</sub>-phos-Mo** catalyst at 353 K with acetonitrile and at 383 K with toluene led to styrene oxide as the major product (Table 1, entries 21 and 23), which was remarkable. Tong et al. reported that polar aprotic solvents, such as acetonitrile, are the most favorable solvents for styrene conversion and those that result in a higher selectivity for benzaldehyde [31], but that was not the case observed here. Tests revealed that styrene conversion was the same for both acetonitrile and toluene. However, selectivity for the desired epoxide was higher for acetonitrile when compared with toluene. Despite that, these observations confirmed that the influence of the solvents in catalysts performance was relevant. Overall, catalysts **MNP<sub>30</sub>-Si-phos-Mo**, **MNP<sub>11</sub>-Si-phos-Mo**, and **MNP<sub>30</sub>-Si<sub>us</sub>-phos-Mo** showed a moderate to low selectivity for epoxide with acetonitrile and toluene as solvents.

Kinetics of benzaldehyde formation in styrene epoxidation with acetonitrile as solvent, was also studied (Figure 4). Results showed that with the **MNP<sub>30</sub>-Si-phos-Mo** catalyst, formation of the epoxide and benzaldehyde occurred simultaneously in the first hours of reaction. However, after 8 h of reaction epoxide yield decreased and benzaldehyde yield increased concomitantly until the end of the reaction, as shown in Figure 4, by interconversion of the epoxide into benzaldehyde through oxidative cleavage mechanism as already reported [28].

**Table 1.** Catalytic epoxidation of *cis*-cyclooctene and styrene using **MNP<sub>30</sub>-Si-phos-Mo**, **MNP<sub>11</sub>-Si-phos-Mo**, and **MNP<sub>30</sub>-Si<sub>us</sub>-phos-Mo** as catalysts.

Entry	Reaction <sup>[a]</sup>	Catalyst	Solvent	Temp. (K)	Conv. <sup>[b]</sup> (%)	Yield <sup>[b]</sup> (%)	Select. <sup>[c]</sup> (%)
1		<b>MNP<sub>30</sub>-Si-phos-Mo</b>	CH <sub>3</sub> CN	353	97	97	100
2			Toluene	353	97	97	100
3			Toluene	383	75	75	100
4			Decane	393	53	53	100
5		<b>MNP<sub>11</sub>-Si-phos-Mo</b>	CH <sub>3</sub> CN	353	92	92	100
6			Toluene	353	99	99	100
7			Toluene	383	99	99	100
8			Decane	393	85	85	100
9		<b>MNP<sub>30</sub>-Si<sub>us</sub>-phos-Mo</b>	CH <sub>3</sub> CN	353	83	83	100
10			Toluene	353	99	99	100
11			Toluene	383	87	87	100
12			Decane	393	52	52	100
13		<b>MNP<sub>30</sub>-Si-phos-Mo</b>	CH <sub>3</sub> CN	353	100	38	38 <sup>[d]</sup>
14			Toluene	353	99	12	12 <sup>[d]</sup>
15			Toluene	383	100	39	39 <sup>[d]</sup>
16			Decane	393	100	27	27 <sup>[d]</sup>
17		<b>MNP<sub>11</sub>-Si-phos-Mo</b>	CH <sub>3</sub> CN	353	100	17	17 <sup>[d]</sup>
18			Toluene	353	100	5	5 <sup>[d]</sup>
19			Toluene	383	100	19	19 <sup>[d]</sup>
20			Decane	393	100	5	5 <sup>[d]</sup>
21		<b>MNP<sub>30</sub>-Si<sub>us</sub>-phos-Mo</b>	CH <sub>3</sub> CN	353	100	72	72 <sup>[d]</sup>
22			Toluene	353	96	7	8 <sup>[d]</sup>
23			Toluene	383	100	54	54 <sup>[d]</sup>
24			Decane	393	99	26	26 <sup>[d]</sup>

<sup>[a]</sup> All reactions were carried out in the presence of 200 mol% oxidant (*tert*-butyl hydroperoxide (tbhp)) and 1 mol% of Mo catalyst relatively to amount of substrate (100 mol%); <sup>[b]</sup> Calculated after 24 h, unless otherwise stated; <sup>[c]</sup> Calculated as "Yield of epoxide"/"Conversion" × 100%; <sup>[d]</sup> In all experiments benzaldehyde formed as by-product.

**Figure 4.** Styrene oxide (closed symbols) and benzaldehyde yield (open symbols) with acetonitrile (a) and toluene (b) as solvents at 353 K.

The performance of the catalysts **MNP<sub>30</sub>-Si-phos-Mo** and **MNP<sub>11</sub>-Si-phos-Mo** agreed with studies carried out with other catalysts based on metallic precursors coordinated to magnetic nanoparticles [32,33]. Those studies revealed that the longer the reaction time, the greater the selectivity for secondary products. This may be due to the presence of a high

amount of oxidant, which reacts with the epoxide that has been formed at the beginning of the reaction.

According to these results, it was found that the ideal conditions for the formation of a higher amount of epoxide, thus minimizing the amount of benzaldehyde were with acetonitrile as solvent in shorter reactions, such as 8 h of reaction, as we could observe for catalyst **MNP<sub>30</sub>-Si-phos-Mo** in Figure 4a (black line, closed symbols). These results agree with those reported by Tong et al. [31].

Reaction temperature was another relevant variable that was very important and influenced benzaldehyde formation in styrene oxidation. Tests with catalysts **MNP<sub>30</sub>-Si-phos-Mo** and **MNP<sub>11</sub>-Si-phos-Mo** revealed that in the presence of the same solvent (toluene), the higher the temperature, the higher the epoxide yield. For catalyst **MNP<sub>30</sub>-Si-phos-Mo** the epoxide yield increased from 12% to 39% at 353 K and 383 K, respectively (Table 1, entries 14 and 15), while under the same conditions, for catalyst **MNP<sub>11</sub>-Si-phos-Mo** the epoxide yield increased from 5% to 19% (Table 1, entries 18 and 19) as we can observe in Figure 5. With these results we can state that an increase in the reaction temperature facilitates the epoxide formation in the presence of catalyst **MNP<sub>30</sub>-Si-phos-Mo** but only in the first minutes of reaction (Figure 5). These results confirmed that the cleavage of C=C bond was higher at lower temperature and the epoxidation competes more favorably against C=C cleavage at higher temperature, as reported in literature [34].

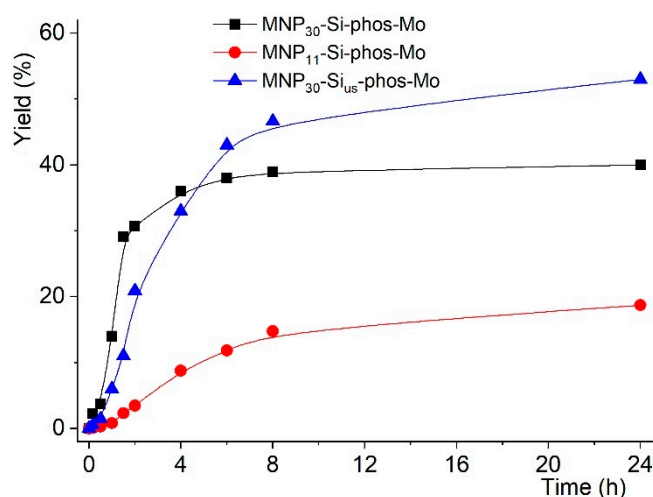
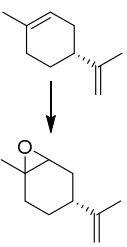
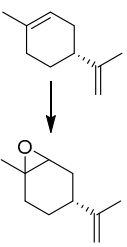
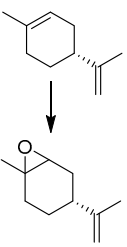
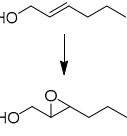
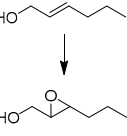
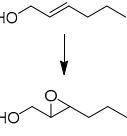


Figure 5. Styrene oxide yield with toluene as solvent at 383 K.

The same was observed for catalyst **MNP<sub>30</sub>-Si<sub>us</sub>-phos-Mo** under similar reaction conditions (Figure 5). However, an increase of reaction temperature from 383 K to 393 K, and changing the reaction solvent from toluene to decane, enabled a decrease of epoxide yield reaching only 26% yield for that product (Table 1, entry 24). For the **MNP<sub>30</sub>-Si-phos-Mo** and **MNP<sub>11</sub>-Si-phos-Mo** counterparts the same trend was observed. In those cases, only 27% and 5% styrene oxide yield were obtained, respectively under similar reaction conditions (Table 1, entries 16 and 20).

Because *R*(+)-limonene is a substrate holding two unsaturated C=C bonds, two different epoxides are feasible: the endo- and the exocyclic isomers. The endocyclic isomer was the sole epoxide formed by all catalysts across all the tests made (Table 2, entries 1–12). It could be anticipated that the exocyclic epoxide would not be formed given that it will be formed on a terminal olefin and therefore not activated for reactivity.

**Table 2.** Catalytic epoxidation of *R*-(+)-limonene and *trans*-hex-2-en-1-ol using **MNP<sub>30</sub>-Si-phos-Mo**, **MNP<sub>11</sub>-Si-phos-Mo**, and **MNP<sub>30</sub>-Si<sub>us</sub>-phos-Mo** as catalysts.

Entry	Reaction <sup>[a]</sup>	Catalyst	Solvent	Temp. (K)	Conv. <sup>[b]</sup> (%)	Yield <sup>[b]</sup> (%)	Select. <sup>[c]</sup> (%)
1		<b>MNP<sub>30</sub>-Si-phos-Mo</b>	CH <sub>3</sub> CN	353	99	65	65 <sup>[d]</sup>
2			Toluene	353	99	74	74 <sup>[d]</sup>
3			Toluene	383	100	96	99 <sup>[d]</sup>
4			Decane	393	99	86	87 <sup>[d]</sup>
5		<b>MNP<sub>11</sub>-Si-phos-Mo</b>	CH <sub>3</sub> CN	353	100	78	78 <sup>[d]</sup>
6			Toluene	353	100	87	87 <sup>[d]</sup>
7			Toluene	383	100	88	88 <sup>[d]</sup>
8			Decane	393	99	88	88 <sup>[d]</sup>
9		<b>MNP<sub>30</sub>-Si<sub>us</sub>-phos-Mo</b>	CH <sub>3</sub> CN	353	88	75	85 <sup>[d]</sup>
10			Toluene	353	81	73	90 <sup>[d]</sup>
11			Toluene	383	97	92	95 <sup>[d]</sup>
12			Decane	393	76	63	83 <sup>[d]</sup>
13		<b>MNP<sub>30</sub>-Si-phos-Mo</b>	CH <sub>3</sub> CN	353	95	65	70 <sup>[e]</sup>
14			Toluene	353	97	78	80 <sup>[e]</sup>
15			Toluene	383	99	82	83 <sup>[e]</sup>
16			Decane	393	95	76	80 <sup>[e]</sup>
17		<b>MNP<sub>11</sub>-Si-phos-Mo</b>	CH <sub>3</sub> CN	353	86	56	65 <sup>[e]</sup>
18			Toluene	353	98	85	86 <sup>[e]</sup>
19			Toluene	383	100	93	93 <sup>[e]</sup>
20			Decane	393	99	84	85 <sup>[e]</sup>
21		<b>MNP<sub>30</sub>-Si<sub>us</sub>-phos-Mo</b>	CH <sub>3</sub> CN	353	100	50	50 <sup>[e]</sup>
22			Toluene	353	100	50	50 <sup>[e]</sup>
23			Toluene	383	96	89	93 <sup>[e]</sup>
24			Decane	393	98	97	99 <sup>[e]</sup>

<sup>[a]</sup> All reactions were carried out in the presence of 200 mol% oxidant (tbhp) and 1 mol% of Mo catalyst relatively to amount of substrate (100 mol%); <sup>[b]</sup> Calculated after 24 h, unless otherwise stated; <sup>[c]</sup> Calculated as "Yield of epoxide"/"Conversion" × 100%; <sup>[d]</sup> In all experiments β-terpineol formed as by-product; <sup>[e]</sup> In all experiments α-hydroxyketone formed as by-product.

Substrate conversion with catalyst **MNP<sub>30</sub>-Si-phos-Mo** gave the best results, with almost 100% conversion under all the tested conditions (Table 2, entries 1–4). The catalyst **MNP<sub>11</sub>-Si-phos-Mo** showed to be efficient in *R*-(+)-limonene epoxidation at a lower temperature (353 K) with acetonitrile giving rise to a 100% conversion, (Table 2, entry 5). The results at higher temperature with this catalyst were quite good as well with the same level of conversion and higher product selectivity (Table 2, entries 6–8). On the other hand, the catalyst **MNP<sub>30</sub>-Si<sub>us</sub>-phos-Mo** was less efficient in *R*-(+)-limonene epoxidation with toluene at lower temperature (353 K) or with decane at 393 K leading to 81% and 76% of conversion, respectively (Table 2, entries 10 and 12). However, reactions with this catalyst at 353 K in acetonitrile and at 383 K in toluene revealed to be the ideal conditions for substrate conversion, achieving 88% and 97% respectively (Table 2, entries 9 and 11). Regarding product selectivity towards the epoxide, catalyst **MNP<sub>30</sub>-Si<sub>us</sub>-phos-Mo** evidenced the best overall performance by showing a minimum epoxide selectivity of 83% obtained for the least performing conditions (Table 2, entry 12). Despite this, high epoxide selectivity values were reached by all catalysts across all tested reaction conditions. For catalyst **MNP<sub>30</sub>-Si<sub>us</sub>-phos-Mo** the silica coating of magnetic nanoparticles by ultrasonication led to less aggregated particles that allowed a better performance, although marginally, concerning product selectivity in *R*-(+)-limonene epoxidation.

All catalysts converted the allylic alcohol *trans*-hex-2-en-1-ol very efficiently towards its epoxide with quite good conversions and selectivity towards the epoxide (Table 2, entries 13–24). The obtained epoxide yields (and selectivity) were found to be sensitive to the solvent or reaction temperature. Namely, for reactions with toluene and decane

the **MNP<sub>30</sub>-Si-phos-Mo** and **MNP<sub>11</sub>-Si-phos-Mo** catalysts were more active than when acetonitrile was used (Table 2, entries 14–16 and 18–20). The same was not observed with catalyst **MNP<sub>30</sub>-Si<sub>us</sub>-phos-Mo** (Table 2, entries 22–24), where substrate conversion in acetonitrile was the highest. However, epoxide selectivity was maximized for catalyst **MNP<sub>30</sub>-Si<sub>us</sub>-phos-Mo** when running the reaction using decane as solvent and at 393 K (Table 2, entry 24). In this case, after only 2 h of reaction the epoxide selectivity reached 99%. In parallel, however, there seemed to occur degradation of the epoxide yielding the  $\alpha$ -hydroxyketone derivative (Figure 6), which was formed by a ring-opening reaction of the epoxide [35].

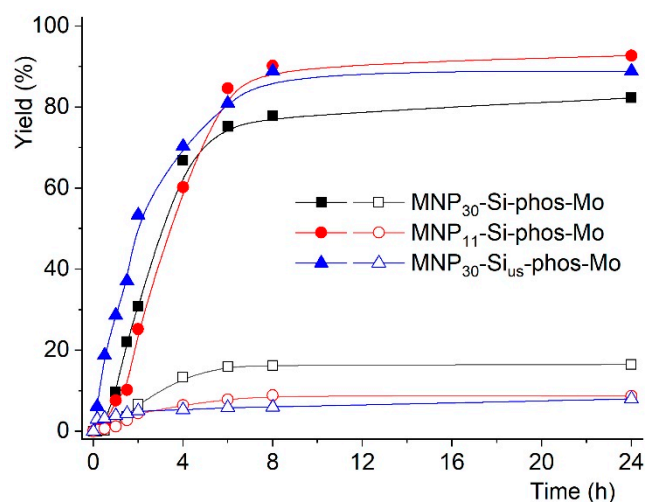


**Figure 6.** Reaction kinetics of *trans*-hex-2-en-1-ol epoxidation, in toluene at 383 K, concerning yield of the epoxide (closed symbols) and  $\alpha$ -hydroxy ketone (open symbols) products.

Kinetic profiling of *trans*-hex-2-en-1-ol epoxidation (Figure 6) showed that all catalysts presented quicker and higher conversion profiles towards the corresponding epoxide in the first hours of reaction and when the reaction temperature was higher, namely, 383 K or 393 K, or when the solvent was toluene, as already mentioned before.

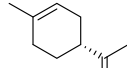
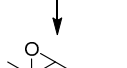
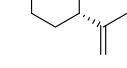
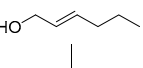
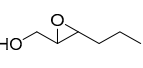
These results agreed with literature reports using a vanadium catalyst coordinated to a Schiff base immobilized in iron oxide ( $\text{Fe}_3\text{O}_4$ ) magnetic nanoparticles, in oxidation catalysis of allylic alcohols, including *trans*-hex-2-en-1-ol, in the presence of *tbhp* as oxidant agent. According to that report, the catalyst was very efficient in substrate conversion, reaching 100%, only after a few hours of reaction [36].

Reusability of the **MNP<sub>30</sub>-Si-phos-Mo**, **MNP<sub>11</sub>-Si-phos-Mo**, and **MNP<sub>30</sub>-Si<sub>us</sub>-phos-Mo** catalysts was also performed, by conducting studies with *cis*-cyclooctene, *R*-(+)-limonene and *trans*-hex-2-en-1-ol across three catalytic runs, to test the stability of the catalysts.

Results revealed that catalysts maintained their catalytic activity being moderate to high after three catalytic cycles, in most of the tested conditions (Table 3).

For *cis*-cyclooctene epoxidation with catalyst **MNP<sub>11</sub>-Si-phos-Mo** it was possible to obtain quite good results after three catalytic cycles, with conversions between 68% and 99%, overall (Table 3, entries 5–8). On the other hand, catalytic activity of catalysts **MNP<sub>30</sub>-Si-phos-Mo** and **MNP<sub>30</sub>-Si<sub>us</sub>-phos-Mo** decreased across the three cycles (Table 3, entries 1–4 and 9–12), although one exception was observed for **MNP<sub>30</sub>-Si-phos-Mo** catalyst using toluene as solvent at 353 K (Table 3, entry 2).

**Table 3.** Reusability of catalysts **MNP<sub>30</sub>-Si-phos-Mo**, **MNP<sub>11</sub>-Si-phos-Mo**, and **MNP<sub>30</sub>-Si<sub>us</sub>-phos-Mo** in different reaction conditions.

Entry	Reaction <sup>[a]</sup>	Catalyst	Solvent	Temp. (K)	Conv. <sup>[b,c]</sup> (%)
1		<b>MNP<sub>30</sub>-Si-phos-Mo</b>	CH <sub>3</sub> CN	353	97/85/70
2			Toluene	353	97/96/96
3			Toluene	383	75/64/53
4			Decane	393	53/36/18
5		<b>MNP<sub>11</sub>-Si-phos-Mo</b>	CH <sub>3</sub> CN	353	92/72/70
6			Toluene	353	99/82/78
7			Toluene	383	99/99/98
8			Decane	393	85/73/68
9		<b>MNP<sub>30</sub>-Si<sub>us</sub>-phos-Mo</b>	CH <sub>3</sub> CN	353	83/86/40
10			Toluene	353	99/99/81
11			Toluene	383	87/49/35
12			Decane	393	52/39/17
13		<b>MNP<sub>30</sub>-Si-phos-Mo</b>	CH <sub>3</sub> CN	353	99/90/72
14			Toluene	353	99/97/37
15			Toluene	383	100/100/94
16			Decane	393	99/31/27
17		<b>MNP<sub>11</sub>-Si-phos-Mo</b>	CH <sub>3</sub> CN	353	100/99/99
18			Toluene	353	100/99/99
19			Toluene	383	100/100/100
20			Decane	393	99/99/99
21		<b>MNP<sub>30</sub>-Si<sub>us</sub>-phos-Mo</b>	CH <sub>3</sub> CN	353	88/53/13
22			Toluene	353	81/45/10
23			Toluene	383	97/49/47
24			Decane	393	76/63/29
25		<b>MNP<sub>30</sub>-Si-phos-Mo</b>	CH <sub>3</sub> CN	353	95/95/86
26			Toluene	353	97/95/89
27			Toluene	383	99/96/93
28			Decane	393	95/92/91
29		<b>MNP<sub>11</sub>-Si-phos-Mo</b>	CH <sub>3</sub> CN	353	86/67/34
30			Toluene	353	98/87/30
31			Toluene	383	100/100/63
32			Decane	393	99/99/79
33		<b>MNP<sub>30</sub>-Si<sub>us</sub>-phos-Mo</b>	CH <sub>3</sub> CN	353	100/68/73
34			Toluene	353	100/99/44
35			Toluene	383	96/98/85
36			Decane	393	98/98/96

<sup>[a]</sup> All reactions were conducted in the presence of 200 mol% oxidant (tbhp) and 1 mol% of Mo catalyst relatively to amount of substrate (100 mol%); <sup>[b]</sup> Calculated after 24 h, <sup>[c]</sup> values for 1st to 3rd cycles.

In the epoxidation studies conducted with *R*-(+)-limonene, catalyst **MNP<sub>11</sub>-Si-phos-Mo** showed a very high catalytic performance, around 100%, even after three cycles under all tested conditions. Figure 7 shows the average kinetics across the three catalytic cycles for substrate consumption and epoxide yield. The small error bars denote that not only were both the final conversion and yield not affected by much but the whole kinetics was unaffected as well, which was relevant. It should also be mentioned that two diastereomers of the epoxide were formed with a preference for the *trans* one. As evidenced in Figure 7b, that trend was kept constant across the recycling tests with little variation.

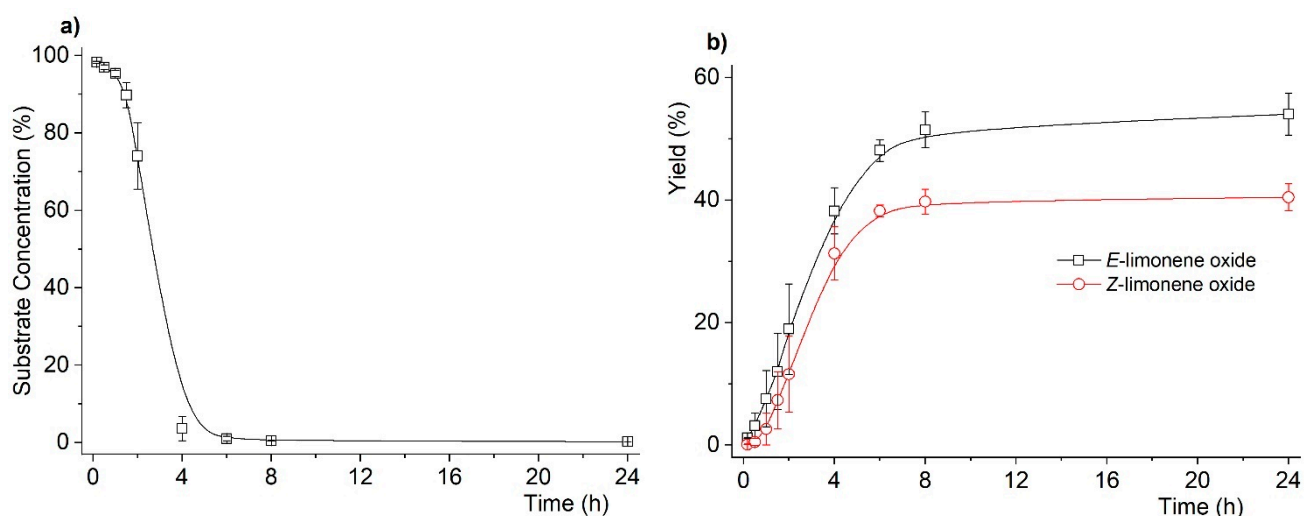


**Figure 7.** *R*-(+)-Limonene conversion (a) and limonene oxide yield (b) for **MNP<sub>11</sub>-Si-phos-Mo** catalyst at 383 K across three catalytic cycles. The data points represent the average values from the three runs and the error bars account for the observed variations. In (b), the limonene oxide yield plot reports the kinetics for the formation of both *cis* (*Z*) and *trans* (*E*) diastereomers of limonene oxide.

For **MNP<sub>30</sub>-Si-phos-Mo** catalyst the catalytic activity decreased significantly after three cycles overall, most dramatic at high temperature (Table 3, entry 16). Similarly, reusability tests using catalyst **MNP<sub>30</sub>-Si<sub>us</sub>-phos-Mo** also showed a significant loss of catalytic activity after the first cycle for all the tested conditions (Table 3, entries 21–24), under all tested conditions.

In the study of *trans*-hex-2-en-1-ol epoxidation, catalyst **MNP<sub>30</sub>-Si-phos-Mo** proved to have a better performance than the other catalysts whose catalytic activity remained very high and almost constant during all the three cycles, for most cases (Table 3, entries 25–28). The same trend was not followed by catalyst **MNP<sub>30</sub>-Si<sub>us</sub>-phos-Mo** who showed some performance loss across recycling experiments.

This behavior with performance decrease was also observed for **MNP<sub>11</sub>-Si-phos-Mo** catalyst since its catalytic activity decreased as well (Table 3, entries 29–32). Possible reasons for this may be related with increasing particle aggregation in these catalysts across the recycling tests, which will lead to their concomitant deactivation.

It should also be mentioned for catalyst **MNP<sub>11</sub>-Si-phos-Mo** that both temperature and solvent choice were found to be critical concerning activity decrease in recycling experiments for *trans*-hex-2-en-1-ol epoxidation, which promoted lower substrate conversion in the third cycle (Table 3, entries 29–32). Again, this catalyst having the smaller particles was the most prone to deactivation.

Stability of the catalysts was evaluated through leaching test of the active species into the reaction media. From the kinetics observed in olefin epoxidation with catalysts **MNP<sub>11</sub>-Si-phos-Mo**, **MNP<sub>30</sub>-Si-phos-Mo**, and **MNP<sub>30</sub>-Si<sub>us</sub>-phos-Mo**, a catalytic cycle was run with different substrates and the catalyst separated after 2 h of reaction. Afterwards, the reaction was kept running without the catalyst to evaluate leaching of Mo species to the slurry. The experimental conditions were chosen considering the best performance of the catalysts.

Figure S5a shows the kinetics of these experiments with *trans*-hex-2-en-1-ol at 353 K in toluene with the **MNP<sub>11</sub>-Si-phos-Mo** catalyst, removed after 2 h. As that figure shows, conversion achieved only 59% instead of proceeding up till 98%. It confirmed that the reaction stopped, implying that there was no leaching of Mo-active species to the reaction medium.

The same test was performed for the remaining catalysts, **MNP<sub>30</sub>-Si-phos-Mo** and **MNP<sub>30</sub>-Si<sub>us</sub>-phos-Mo**, under the same conditions—*cis*-cyclooctene epoxidation at 353 K with toluene (Figure 8 and Figure S5b). Once the catalysts were removed, substrate conversion progressed little till 24 h reaction time as opposed to the reaction in the presence

of the catalysts. Such results demonstrated that the MNP materials were robust and true heterogeneous catalysts.

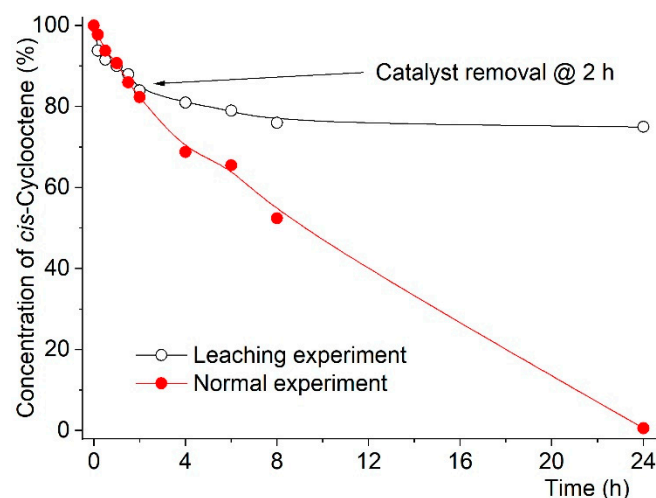


**Figure 8.** Leaching experiment reaction kinetics of substrate consumption in toluene at 353 K for *cis*-cyclooctene epoxidation in the presence of **MNP<sub>30</sub>-Si<sub>us</sub>-phos-Mo** catalyst. In the leaching experiment the catalyst was removed after 2 h reaction time.

Efficiency of the catalysts was also evaluated by changing the amount of oxidant, *tert*-butylhydroperoxide (tbhp), from 200 mol% relatively to olefin, as described in literature [37,38], down to 150 and 100 mol%, i.e., till reaching stoichiometric oxidant/substrate ratio. Catalyst's efficiency was tested for *cis*-cyclooctene and *R*-(+)-limonene epoxidation at 353 K and 383 K with toluene as solvent (Table 4). These reaction conditions were chosen considering the good performance of catalysts as shown in Tables 1 and 2.

**Table 4.** *cis*-Cyclooctene and *R*-(+)-limonene epoxidation with different amounts of oxidant, *tert*-butylhydroperoxide (tbhp), in toluene and in the presence of catalysts **MNP<sub>11</sub>-Si-phos-Mo**, **MNP<sub>30</sub>-Si-phos-Mo**, and **MNP<sub>30</sub>-Si<sub>us</sub>-phos-Mo**.

Entry	Reaction <sup>[a]</sup>	Catalyst	Temp. (K)	Conv. <sup>[b]</sup> (%)			Select. <sup>[b,c]</sup> (%)		
				100 <sup>[d]</sup>	150 <sup>[d]</sup>	200 <sup>[d]</sup>	100 <sup>[d]</sup>	150 <sup>[d]</sup>	200 <sup>[d]</sup>
1		<b>MNP<sub>30</sub>-Si-phos-Mo</b>	353	99	99	97	100	100	100
2			383	99	99	75	100	100	100
3		<b>MNP<sub>11</sub>-Si-phos-Mo</b>	353	54	28	99	100	100	100
4			383	93	100	99	100	100	100
5		<b>MNP<sub>30</sub>-Si<sub>us</sub>-phos-Mo</b>	353	37	37	99	100	100	100
6			383	84	86	87	100	100	100
7		<b>MNP<sub>30</sub>-Si-phos-Mo</b>	353	46	60	99	91 <sup>[e]</sup>	92 <sup>[e]</sup>	74 <sup>[e]</sup>
8			383	99	57	100	65 <sup>[e]</sup>	92 <sup>[e]</sup>	99 <sup>[e]</sup>
9		<b>MNP<sub>11</sub>-Si-phos-Mo</b>	353	64	89	100	93 <sup>[e]</sup>	90 <sup>[e]</sup>	87 <sup>[e]</sup>
10			383	81	97	100	94 <sup>[e]</sup>	93 <sup>[e]</sup>	88 <sup>[e]</sup>
11		<b>MNP<sub>30</sub>-Si<sub>us</sub>-phos-Mo</b>	353	27	41	81	87 <sup>[e]</sup>	88 <sup>[e]</sup>	90 <sup>[e]</sup>
12			383	100	76	97	87 <sup>[e]</sup>	92 <sup>[e]</sup>	95 <sup>[e]</sup>

<sup>[a]</sup> All reactions were carried out in the presence of different amounts of mol% of oxidant (tbhp) and 1 mol% of Mo catalyst relatively to 100 mol% of substrate in toluene; <sup>[b]</sup> Calculated after 24 h; <sup>[c]</sup> Calculated as "Yield of epoxide"/"Conversion" × 100%; <sup>[d]</sup> Amount of mol% oxidant (tbhp) used; <sup>[e]</sup> In all experiments  $\beta$ -terpineol formed as by-product.

For *cis*-cyclooctene epoxidation, all systems performed at their best when the tbhp ratio was set to 200 mol%. Although product selectivity towards the epoxide product was

not affected the substrate conversion level vs. *tbhp* ratio was found to vary drastically only for some cases (Table 4, entries 3 and 5).

In the epoxidation of *R*-(+)-limonene, the catalytic system's performance followed the same trend by reaching higher substrate conversion at 200 mol% *tbhp* ratio. Catalyst **MNP<sub>30</sub>-Si-phos-Mo** at a lower temperature, 353 K, was very dependent on the amount of oxidant, since epoxide conversion increases with the increase of the amount of *tbhp* (Table 4, entry 7). However, at a higher temperature, 383 K, conversion was practically complete (99% of conversion) with a lower amount of oxidant (100 mol% of *tbhp*) (Table 4, entry 8). Despite the good results for conversion at a higher temperature, selectivity was found to be dependent on the oxidant ratio, meaning that there are side reactions consuming substrate and not leading to the epoxide.

In what concerns selectivity, values remained generally at very high levels always above 87%. The exceptions were observed for catalyst **MNP<sub>30</sub>-Si-phos-Mo** (Table 4, entries 7 and 8), which evidenced a drop to 74% when using 200 mol% *tbhp* at 353 K and experienced a selectivity drop to 65% when using stoichiometric *tbhp* ratio at 383 K.

The same was observed for catalyst **MNP<sub>11</sub>-Si-phos-Mo** (Table 4, entries 9 and 10), where the amount of the oxidant was also a very important factor for substrate conversion. In terms of selectivity that dependence was not observed to a great extent with levels being kept constant.

The results obtained for catalyst **MNP<sub>30</sub>-Si<sub>us</sub>-phos-Mo** revealed that the amount of oxidant was important to its performance. Furthermore, they also showed that there were side reactions that rendered the catalytic process some inefficiency, most probably concerning decomposition of *tbhp* without leading to any oxidation products.

Kinetics of the reactions was also influenced by *tbhp* ratio. As can be seen in Figure 9, *cis*-cyclooctene epoxidation at 383 K in toluene as solvent with different amounts of oxidant (100 mol%, 150 mol%, and 200 mol%) and in the presence of catalyst **MNP<sub>11</sub>-Si-phos-Mo**. The reaction kinetics became faster on going from 100 mol% to 150 mol% and then decreased slightly when further increasing the *tbhp* amount. This observation is most probably showing the inefficiency of the catalytic system due to the already mentioned side-reactions for *tbhp* decomposition, which slow down the reaction as observed.

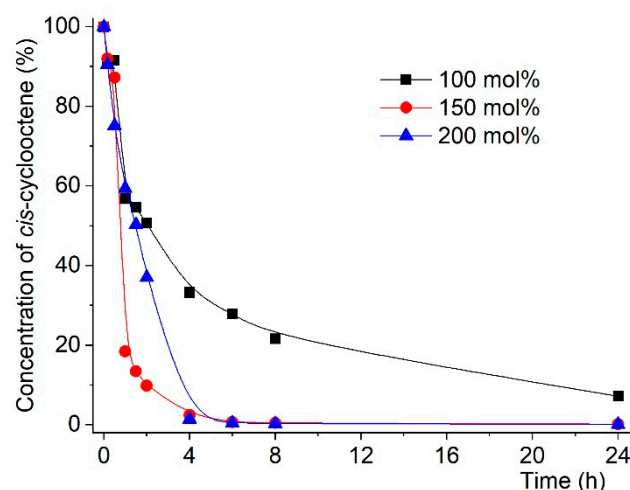


**Figure 9.** Kinetics of *cis*-cyclooctene epoxidation in the presence of **MNP<sub>11</sub>-Si-phos-Mo** catalyst in toluene at 383 K, and with different *tert*-butylhydroperoxide (*tbhp*): substrate ratios.

The systems discussed in this work were also benchmarked against related systems found in the literature. Table 5 collects some of the data found for systems already published alongside those reported here for *cis*-cyclooctene and styrene epoxidation. As can be seen, for the former all the catalysts reported here performed at the same level or were even better than their counterparts.

**Table 5.** Comparison of catalytic performance between this work and previously reported systems from the literature.

Entry	Catalyst	Substrate	Oxidant	Temp (K)	Conv. (%)	Epoxide Select. (%)	Ref.
1	<b>Fe<sub>3</sub>O<sub>4</sub>@SiO<sub>2</sub>@PTMS@Mel-Naph-VO</b>	<i>cis</i> -cyclooctene	tbhp	353	80	100 (8 h)	[36]
2		styrene			56	58 (3 h)	
3	<b>Fe<sub>3</sub>O<sub>4</sub>/SiO<sub>2</sub>/NH<sub>2</sub>-MnTCPP(OAc)</b>	<i>cis</i> -cyclooctene	H <sub>2</sub> O <sub>2</sub>	303	85	100 (3 h)	[39]
4		styrene			74	78 (3 h)	
5	<b>MNP@PMA-SB-Mo</b>	<i>cis</i> -cyclooctene	tbhp	357	98	100 (1 h)	[40]
6		styrene			92	72 (3 h)	
7	<b>Fe<sub>3</sub>O<sub>4</sub>@SiO<sub>2</sub>-dendrimer-Mo</b>	<i>cis</i> -cyclooctene	tbhp	323	96	99 (1 h)	[41]
8		styrene			92	98 (2 h)	
9	<b>MnFe<sub>2</sub>O<sub>4</sub>-Mo(VI)</b>	<i>cis</i> -cyclooctene	tbhp	368	99	100 (10 min)	[42]
10		styrene			94	56 (15 min)	
11	<b>MNP<sub>30</sub>-Si-phos-Mo</b>	<i>cis</i> -cyclooctene	tbhp	383	75	100 (24 h)	This work
12		styrene			99	39 (24 h)	
13	<b>MNP<sub>11</sub>-Si-phos-Mo</b>	<i>cis</i> -cyclooctene	tbhp	383	99	99 (24 h)	This work
14		styrene			100	19 (24 h)	
15	<b>MNP<sub>30</sub>-Si<sub>us</sub>-phos-Mo</b>	<i>cis</i> -cyclooctene	tbhp	383	87	100 (24 h)	This work
16		styrene			100	54 (24 h)	

In the case of styrene epoxidation, the catalysts reported here were found to match the activity of the other systems in terms of substrate conversion. However, epoxide selectivity was disappointing with benzaldehyde being the major product, with the best selectivity record (Table 5, entry 16) almost matching the worst result (Table 5, entry 10) found for the related systems. Overall, the obtained results seemed to be aligned with those found for similar systems.

### 3. Materials and Methods

#### 3.1. General

All reagents were obtained from Aldrich (St. Louis, MO, USA) and used without any further purification procedures. Standard procedures were followed for purifying commercial grade solvents, comprising drying, deoxygenating, distillation under nitrogen and keeping over 4 Å molecular sieves. The complex [MoI<sub>2</sub>(CO)<sub>3</sub>(CH<sub>3</sub>CN)<sub>2</sub>] [27,43] and the ligand 4-(diphenylphosphino)benzoyl chloride (**phosCl**) [24] were prepared according to literature procedures.

The iron oxide magnetic nanoparticles (MNP), and the silica coated iron oxide nanoparticles were also prepared according to literature procedures [13,20,21].

FTIR spectra were measured as KBr pellets on a Thermo Nicolet 6700 (Waltham, MA, USA) in the 400–4000 cm<sup>-1</sup> range using 4 cm<sup>-1</sup> resolution. Powder XRD measurements were done on a Philips Analytical PW 3050/60 X'Pert PRO (theta/2 theta) (Almelo, The Netherlands) equipped with X'Celerator detector and with automatic data acquisition (X'Pert Data Collector (v2.0b) software), using a monochromatized CuKα radiation as incident beam. <sup>1</sup>H and <sup>13</sup>C solution NMR spectra were obtained with a Bruker Avance 400 spectrometer (Billerica, MA, USA).

Microanalyses (C, P, H, Mo) were performed by C.A.C.T.I. at the University of Vigo, Spain.

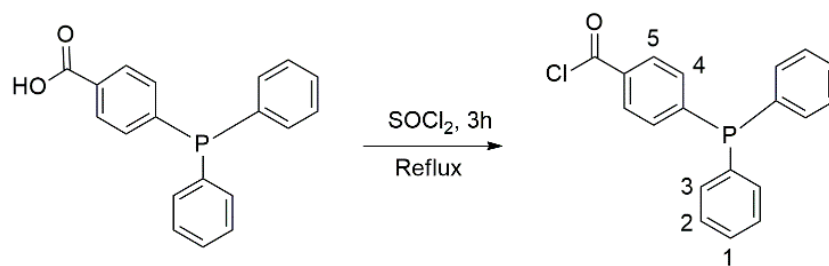
The SEM images and EDX analyses were done on a FEG-SEM (Field Emission Gun Scanning Electron Microscope) from JEOL, model JSM-7001F (Akishima, Tokyo, Japan).

The TEM images were captured on a Hitachi microscope, model H-1800 (Tokyo, Japan) with a LaB<sub>6</sub> filament and an acceleration tension of 200 kV, at Microlab, Instituto Superior Técnico, Lisbon. For size distribution calculation approximately 220 nanoparticles from **MNP<sub>11</sub>** and **MNP<sub>30</sub>** samples were measured.

### 3.1.1. Methods

#### Synthesis of 4-(diphenylphosphino)benzoyl Chloride (**phosCl**)

SOCl<sub>2</sub> (5 mL) was added to 4-(diphenylphosphino)benzoic acid (0.306 g, 1.00 mmol) and the solution was refluxed under strong stirring for 3 h (Scheme 2). The solution was then vacuum evaporated, and the desired product was obtained as a white powder.



**Scheme 2.** Synthesis of 4-(diphenylphosphino)benzoyl chloride (**phosCl**) ligand.

IV (KBr  $\nu/\text{cm}^{-1}$ ): 3010 (w); 2972 (w); 1773 (m); 1738 (m); 1639 (m); 1619 (s); 1496 (s); 1398 (s); 879 (w); 848 (w); 719 (s); 692 (s).

<sup>1</sup>H RMN (400.13 MHz, CDCl<sub>3</sub>, r.t,  $\delta$  ppm): 8.22 (d, H<sub>5</sub>), 7.87 (t, H<sub>1</sub>), 7.70 (t, H<sub>2</sub>), 7.64 (t, H<sub>4</sub>), 7.55 (d, H<sub>3</sub>).

#### Preparation of **MNP<sub>30</sub>-Si<sub>us</sub>** Material

A suspension of **MNP<sub>30</sub>** (1.00 g) in a mixture of absolute ethanol (100 mL), distilled water (60 mL), and aqueous ammonia (0.6 mL) in a three-neck flask was dispersed under ultrasonication for 1 h at 298 K. A second solution containing TEOS (16.67 mL; 74.66 mmol) in absolute ethanol (40 mL) was prepared by mechanical stirring for 10 min at 298 K. This solution was slowly added to the first dispersed suspension at a rate of 0.5 mL/min. The final mixture was kept under ultrasonication for 12 h at room temperature (298–3030 K). The obtained solid was magnetically separated, washed with distilled water (2  $\times$  10 mL) and ethanol (2  $\times$  10 mL). Finally, the purified product was vacuum-dried at 333 K for 4 h.

**MNP<sub>30</sub>-Si<sub>us</sub>**

IV (KBr  $\nu/\text{cm}^{-1}$ ): 1400 (m); 1092 (vs); 1067 (vs); 575 (m).

#### Preparation of **MNP<sub>30</sub>-Si-phos**, **MNP<sub>30</sub>-Si<sub>us</sub>-phos** and **MNP<sub>11</sub>-Si-phos** Materials

Firstly, 0.150 g of **phosCl** ligand was dissolved in 5 mL of dry dichloromethane and added to 0.300 g of **MNP<sub>30</sub>-Si**, **MNP<sub>30</sub>-Si<sub>us</sub>** or **MNP<sub>11</sub>-Si** in 30 mL of dry toluene. The mixture was stirred at 363 K under N<sub>2</sub> atmosphere for 3 h. The obtained solid material was separated with a magnet, washed several times with toluene (2  $\times$  10 mL) and dichloromethane (2  $\times$  10 mL) and then vacuum dried.

**MNP<sub>30</sub>-Si-phos**

IV (KBr  $\nu/\text{cm}^{-1}$ ): 3134 (m); 1701 (w); 1617 (w); 1400 (w); 1067 (m); 711 (w); 565 (m)

Elemental analysis (%): found C 20.89; H 1.38; P 2.84.

**MNP<sub>30</sub>-Si<sub>us</sub>-phos**

IV (KBr  $\nu/\text{cm}^{-1}$ ): 3009 (w); 1709 (m); 1553 (w); 1410 (m); 1093 (vs); 727 (w); 582 (m)

Elemental analysis (%): found C 24.88; H 1.65; P 3.38.

**MNP<sub>11</sub>-Si-phos**

IV (KBr  $\nu/\text{cm}^{-1}$ ): 3129 (m); 1703 (w); 1654 (w); 1624 (w); 1400 (w); 1115 (w); 713 (w); 668 (w); 560 (m)

Elemental analysis (%): found C 19.62; H 1.30; P 2.66.

### Preparation of MNP<sub>30</sub>-Si-phos-Mo, MNP<sub>30</sub>-Si<sub>us</sub>-phos-Mo, and MNP<sub>11</sub>-Si-phos-Mo Materials

**MoI<sub>2</sub>(CO)<sub>3</sub>(NCMe)<sub>2</sub>** (0.130 g, 0.25 mmol) was dissolved in 5 mL of dry dichloromethane and added to a suspension of **MNP<sub>30</sub>-Si-phos**, **MNP<sub>30</sub>-Si<sub>us</sub>-phos** or **MNP<sub>11</sub>-Si-phos** (0.600 g) in 30 mL of dry toluene. The mixture was stirred at 363 K under nitrogen atmosphere for 3 h. The obtained solid material was separated with a magnet, washed several times with toluene (2 × 10 mL) and dichloromethane (2 × 10 mL) and finally vacuum dried.

#### MNP<sub>30</sub>-Si-phos-Mo

IV (KBr  $\nu/\text{cm}^{-1}$ ): 3112 (m); 2050 (w); 1982 (vw); 1920 (vw); 1617 (m); 1559 (w); 1400 (w); 1115 (w); 668 (w); 565 (m)

Elemental analysis (%): found C 21.30; H 1.37; P 3.05; Mo 1.89.

#### MNP<sub>11</sub>-Si-phos Mo

IV (KBr  $\nu/\text{cm}^{-1}$ ): 3130 (m); 2060 (w); 1992 (vw); 1929 (vw); 1701 (w); 1636 (m); 1400 (m); 1112 (m); 731 (w); 668 (m), 563 (m)

Elemental analysis (%): found C 20.60; H 1.33; P 2.82; Mo 1.75.

#### MNP<sub>30</sub>-Si<sub>us</sub>-phos-Mo

IV (KBr  $\nu/\text{cm}^{-1}$ ): 3120 (w); 2062 (w); 1982 (w); 1929 (w); 1629 (m); 1550 (w); 1400 (m); 1105 (vs); 726 (w); 573 (m)

Elemental analysis (%): found C 26.11; H 1.64; P 3.15; Mo 3.26.

### 3.2. Catalytic Tests

The Mo-containing materials were assessed in the catalytic epoxidation of *cis*-cyclooctene, styrene, *trans*-hex-2-en-1-ol and *R*-(+)-limonene, using *tert*-butylhydroperoxide (tbhp) as oxidant. The catalytic tests were carried out at 328 K, 353 K, 383 K, and 393 K under normal atmosphere in a reactor fitted with a magnetic stirrer and a condenser. Typically experiment the reactor was charged with olefin or allylic alcohol (100 mol%), dibutylether (internal standard), catalyst (1 mol%), oxidant (200 mol%), and 3 mL of solvent (acetonitrile, toluene, or decane).

When testing for catalyst efficiency towards tbhp, the latter was also screened for 100 mol% and 150 mol%. The initial time of the reaction was set by addition of the oxidant. The reactions were monitored by quantitative GC-MS analysis by sampling at 0 min (before addition of oxidant), 10 and 30 min, 1 h, 1 h 30 min then at 2, 4, 6, 8, and 24 h of reaction. Before GC injection, the samples were handled as described previously [25].

When conducting recycling experiments, after each cycle (24 h), the catalyst was washed with dichloromethane several times and dried for 1 h–1 h 30 min, prior to reuse in a new catalytic cycle [23].

## 4. Conclusions

In the present work the synthesis of magnetic iron oxide nanoparticles of different sizes (namely, average size of 11 nm and 30 nm) and synthesized by different methods was reported. The nanoparticles were shelled with a silica layer that conferred them some stability and, concomitantly, allowed them to experience additional surface derivatization. An organic ligand was then anchored to those material's surface, followed by coordination of the [MoI<sub>2</sub>(CO)<sub>3</sub>] fragment to the ligand. The successful synthesis of these organometallic magnetic nanoparticles was verified by evidence from structural characterization.

Catalytic testing of the materials in olefin epoxidation using different substrates yielded very promising results. The tests showed that the catalysts yielded selectively the desired epoxides, except for styrene epoxidation which yielded preferably benzaldehyde. All catalytic systems yielded high levels of performance as given by the epoxide selectivity. For instance, while in the case of *cis*-cyclooctene all catalysts converted this substrate to the corresponding epoxide with absolute selectivity for all the other substrates that was not the case. Except for styrene (mentioned above) limonene and *trans*-hex-2-en-1-ol epoxidation yielded the corresponding epoxides as major products (selectivity above 50%), which demonstrated that the catalytic systems showed adequate chemo- and regioselectivity.

These properties are extremely relevant when developing catalytic systems as to ensure resource and environmental impact optimization.

In addition, the catalysts were found to work under a wide range of temperatures without losing the performance in most of the cases and across consecutive cycles. Catalyst **MNP<sub>30</sub>-Si-phos-Mo** proved to be efficient in the conversion of substrates especially at higher temperatures (383 K) and with toluene as solvent. On the other hand, catalyst **MNP<sub>11</sub>-Si-phos-Mo** kept its catalytic performance during almost all the catalytic experiments that were conducted. The catalytic performance of these catalysts was found to match with previously reported systems also based in magnetic nanoparticles, as discussed. Stability tests revealed that silica coating method was important for good catalyst performance in olefin epoxidation. This was more relevant for the **MNP<sub>30</sub>-Si<sub>us</sub>-phos-Mo** catalyst, whose synthesis protocol yielded less aggregated particles and therefore with higher activity. The performance of the catalytic systems was also found to match that of related systems found in the literature.

We also found strong solvent effects between the use of polar (acetonitrile) and apolar (toluene) solvents under similar reaction conditions, which are currently being addressed by our lab.

**Supplementary Materials:** The following are available online at <https://www.mdpi.com/2073-4344/11/3/380/s1>, Figure S1: XRD powder patterns of all prepared materials starting from **MNP<sub>11</sub>** (a) and **MNP<sub>30</sub>** (b). Indexation of the most relevant magnetite (Fe<sub>3</sub>O<sub>4</sub>) plans is also shown; Figure S2: SEM images of **MNP<sub>30</sub>** (a), **MNP<sub>30</sub>-Si** (b) and **MNP<sub>30</sub>-Si<sub>us</sub>** (c); Figure S3: EDX spectra of **MNP<sub>30</sub>-Si** (a), **MNP<sub>30</sub>-Si-phos-Mo** (b) and the particle size distribution histograms for both **MNP<sub>11</sub>** and **MNP<sub>30</sub>** based on TEM measurements (c); Figure S4: FTIR spectra of **MNP<sub>11</sub>** (a) and **MNP<sub>30</sub>** by mechanical stirring route (b) derived materials. The dotted boxes highlight the  $\nu\text{C}\equiv\text{O}$  modes denoting presence of the [MoI<sub>2</sub>(CO)<sub>3</sub>] moiety; Figure S5: Leaching experiment reaction kinetics of substrate consumption in toluene at 353 K for (a) *trans*-hex-2-en-1-ol using **MNP<sub>11</sub>-Si-phos-Mo** and (b) *cis*-cyclooctene using **MNP<sub>30</sub>-Si<sub>us</sub>-phos-Mo** as catalysts, respectively.

**Author Contributions:** C.I.F.: Investigation, Formal Analysis, Writing—Review and Editing. P.D.V.: Conceptualization, Investigation, Data Curation, and Writing—Review and Editing. C.D.N.: Conceptualization, Methodology, Supervision, Project Administration, and Writing—Review and Editing. All authors have read and agreed to the published version of the manuscript.

**Funding:** This research was funded by Fundação para a Ciência e Tecnologia (FCT), Portugal, is acknowledged for financial support to Centro de Química Estrutural through grants UIDB/00100/2020 and UIDP/00100/2020.

**Conflicts of Interest:** All authors declare no conflict of interests.

## References

1. Ganesh, M.; Ramakrishna, J. Synthetic Organic Transformations of Transition-Metal Nanoparticles as Propitious Catalysts: A Review. *Asian J. Org. Chem.* **2020**, *9*, 1341–1376. [[CrossRef](#)]
2. Duan, M.; Shpter, J.G.; Qi, W.; Yang, S.; Gao, G. Recent progress in magnetic nanoparticles: Synthesis, properties, and applications. *Nanotechnology* **2018**, *29*, 452001. [[CrossRef](#)]
3. Arndt, D.; Gesing, T.M.; Bäumer, M. Surface Functionalization of Iron Oxide Nanoparticles and their Stability in Different Media. *ChemPlusChem* **2012**, *77*, 576–583. [[CrossRef](#)]
4. Kim, D.; Shin, K.; Kwon, S.G.; Hyeon, T. Synthesis and Biomedical Applications of Multifunctional Nanoparticles. *Adv. Mater.* **2018**, *30*, 1802309–1802334. [[CrossRef](#)]
5. Fernandes Cardoso, V.; Francesko, A.; Ribeiro, C.; Bañobre-López, M.; Martins, P.; Lancero-Mendez, S. Advances in Magnetic Nanoparticles for Biomedical Applications. *Adv. Healthcare Mater.* **2018**, *7*, 1700845. [[CrossRef](#)]
6. Zhang, Q.; Yang, X.; Guan, J. Applications of Magnetic Nanomaterials in Heterogeneous Catalysis. *ACS Appl. Nano Mater.* **2019**, *2*, 4681–4697. [[CrossRef](#)]
7. Farooqi, Z.H.; Begum, R.; Nassim, K.; Wu, W.; Irfan, A. Zero valent iron nanoparticles as sustainable nanocatalysts for reduction reactions. *Catal. Rev.* **2020**. [[CrossRef](#)]
8. Chiozzi, V.; Rossi, F. Inorganic–organic core/shell nanoparticles: Progress and applications. *Nanoscale Adv.* **2020**, *2*, 5090–5105. [[CrossRef](#)]

9. Hou, Z.; Liu, Y.; Xu, J.; Zhu, J. Surface engineering of magnetic iron oxide nanoparticles by polymer grafting: Synthesis progress and biomedical applications. *Nanoscale* **2020**, *12*, 14957–14975. [[CrossRef](#)] [[PubMed](#)]
10. Singh, R.; Bhatia, R. Core-shell nanostructures: A simplest two-component system with enhanced properties and multiple applications. *Environ. Geochem. Health* **2020**. [[CrossRef](#)]
11. Plumeré, N.; Ruff, A.; Speiser, B.; Felbmann, V.; Mayer, H.A. Stöber silica particles as basis for redox modifications: Particle shape, size, polydispersity, and porosity. *J. Colloid Interface Sci.* **2012**, *368*, 208–219. [[CrossRef](#)] [[PubMed](#)]
12. Wang, J.; Zheng, S.; Shao, Y.; Liu, J.; Xu, Z.; Zhu, D. Amino-functionalized Fe<sub>3</sub>O<sub>4</sub>@SiO<sub>2</sub> core-shell magnetic nanomaterial as a novel adsorbent for aqueous heavy metals removal. *J. Colloid Interface Sci.* **2010**, *349*, 293–299. [[CrossRef](#)] [[PubMed](#)]
13. Sun, X.; Liu, F.; Sun, L.; Wang, Q.; Ding, Y. Well-Dispersed Fe<sub>3</sub>O<sub>4</sub>/SiO<sub>2</sub> Nanoparticles Synthesized by a Mechanical Stirring and Ultrasonication Assisted Stöber Method. *J. Inorg. Organomet. Polym.* **2012**, *22*, 311–315. [[CrossRef](#)]
14. Shokouhimehr, M.; Piao, Y.; Kim, J.; Jan, Y.; Hyeon, T. A magnetically recyclable nanocomposite catalyst for olefin epoxidation. *Angew. Chem. Int. Ed. Engl.* **2007**, *46*, 7039–7043. [[CrossRef](#)]
15. Pan, Z.; Hua, L.; Qiao, Y.; Yang, H.; Zhao, X.; Feng, B.; Zhu, W. Nanostructured Maghemite-Supported Silver Catalysts for Styrene Epoxidation. *Chin. J. Catal.* **2011**, *32*, 428–435. [[CrossRef](#)]
16. Shen, Y.; Jiang, P.; Wai, P.T.; Gu, Q.; Zhang, W. Recent Progress in Application of Molybdenum-Based Catalysts for Epoxidation of Alkenes. *Catalysts* **2019**, *9*, 31. [[CrossRef](#)]
17. Vasconcelos-Dias, M.; Nunes, C.D.; Vaz, P.D.; Ferreira, P.; Brandão, P.; Felix, V.; Calhorda, M.J. Heptacoordinate tricarbonyl Mo(II) complexes as highly selective oxidation homogeneous and heterogeneous catalysts. *J. Catal.* **2008**, *256*, 301–311. [[CrossRef](#)]
18. Fernandes, C.I.; Stenning, G.B.G.; Taylor, J.D.; Nunes, C.D.; Vaz, P.D. Helical channel mesoporous materials with embedded magnetic iron nanoparticles: Chiral recognition and implications in asymmetric olefin epoxidation. *Adv. Synth. Catal.* **2015**, *357*, 3127–3140. [[CrossRef](#)]
19. Tokudome, Y.; Morimoto, T.; Tarutani, N.; Vaz, P.D.; Nunes, C.D.; Prevot, V.; Stenning, G.B.G.; Takahashi, M. Layered Double Hydroxide Nanoclusters: Aqueous, Concentrated, Stable, and Catalytically Active Colloids toward Green Chemistry. *ACS Nano* **2016**, *10*, 5550–5559. [[CrossRef](#)]
20. Fernandes, C.I.; Carvalho, M.D.; Ferreira, L.P.; Nunes, C.D.; Vaz, P.D. Organometallic Mo complex anchored to magnetic iron oxide nanoparticles as highly recyclable epoxidation catalyst. *J. Organomet. Chem.* **2014**, *760*, 2–10. [[CrossRef](#)]
21. Shylesh, S.; Schweizer, J.; Demeshko, S.; Schunemann, V.; Ernst, S.; Thiel, W.R. Nanoparticle Supported, Magnetically Recoverable Oxodiperoxo Molybdenum Complexes: Efficient Catalysts for Selective Epoxidation Reactions. *Adv. Synth. Catal.* **2009**, *351*, 1789–1795. [[CrossRef](#)]
22. Bui, T.Q.; Ngo, H.T.M.; Tran, H.T. Surface-protective assistance of ultrasound in synthesis of superparamagnetic magnetite nanoparticles and in preparation of mono-core magnetite-silica nanocomposites. *J. Sci. Adv. Mater. Dev.* **2018**, *3*, 323–330. [[CrossRef](#)]
23. Montaña-Priede, J.L.; Coelho, J.P.; Guerrero-Martínez, A.; Peña-Rodríguez, O.; Pal, U. Fabrication of Monodispersed Au@SiO<sub>2</sub> Nanoparticles with Highly Stable Silica Layers by Ultrasound-Assisted Stöber Method. *J. Phys. Chem. C* **2017**, *121*, 9543–9551. [[CrossRef](#)]
24. Ventura, A.C.; Fernandes, C.I.; Saraiva, M.S.; Nunes, T.G.; Vaz, P.D.; Nunes, C.D. Tuning the Surface of Mesoporous Materials Towards Hydrophobicity-Effects in Olefin Epoxidation. *Curr. Inorg. Chem.* **2011**, *1*, 156–165. [[CrossRef](#)]
25. Arzoumanian, H.; Castellanos, N.J.; Martínez, F.O.; Páez-Mozo, E.A.; Ziarelli, F. Silicon-Assisted Direct Covalent Grafting on Metal Oxide Surfaces: Synthesis and Characterization of Carboxylate N,N'-Ligands on TiO<sub>2</sub>. *Eur. J. Inorg. Chem.* **2010**, 1633–1641. [[CrossRef](#)]
26. Vaz, P.D.; Nunes, C.D.; Vasconcelos-Dias, M.; Nolasco, M.M.; Ribeiro-Claro, P.J.A.; Calhorda, M.J. Vibrational Study on the Local Structure of Post-Synthesis and Hybrid Mesoporous Materials: Are There Fundamental Distinctions? *Chem. Eur. J.* **2007**, *13*, 7874–7882. [[CrossRef](#)] [[PubMed](#)]
27. Baker, P.K. Seven-coordinate halocarbonyl complexes of the type [MXY(CO)<sub>3</sub>(NCMe)<sub>2</sub>] (M = Mo, W.; X, Y = halide, pseudo halide) as highly versatile starting materials. *Chem. Soc. Rev.* **1998**, *27*, 125–132. [[CrossRef](#)]
28. Fernandes, C.I.; Silva, N.U.; Vaz, P.D.; Nunes, T.G.; Nunes, C.D. Bio-inspired Mo(II) complexes as active catalysts in homogeneous and heterogeneous olefin epoxidation. *Appl. Catal. A Gen.* **2010**, *384*, 84–93. [[CrossRef](#)]
29. Guo, W.C.; Wang, G.; Wang, Q.; Dong, W.J.; Yang, M.; Huang, X.B.; Yu, J.; Shi, Z. A hierarchical Fe<sub>3</sub>O<sub>4</sub>@P4VP@MoO<sub>2</sub>(acac)<sub>2</sub> nanocomposite: Controlled synthesis and green catalytic application. *J. Mol. Catal. A Chem.* **2013**, *378*, 344–349. [[CrossRef](#)]
30. Huang, X.B.; Guo, W.C.; Wang, G.; Yang, M.; Wang, Q.; Zhang, X.X.; Feng, Y.H.; Shi, Z.; Li, C.G. Synthesis of Mo-Fe<sub>3</sub>O<sub>4</sub>@SiO<sub>2</sub>@P4VP core-shell-shell structured magnetic microspheres for alkene epoxidation reactions. *Mater. Chem. Phys.* **2012**, *135*, 985–990. [[CrossRef](#)]
31. Tong, J.; Cai, X.; Wang, H.; Zhang, Q. Improvement of catalytic activity in selective oxidation of styrene with H<sub>2</sub>O<sub>2</sub> over spinel Mg-Cu ferrite hollow spheres in water. *Mater. Res. Bull.* **2014**, *55*, 205–211. [[CrossRef](#)]
32. Wilson, K.; Lee, A.F. Catalyst design for biorefining. *Philos. Trans. R. Soc. A* **2016**, *374*, 20150081. [[CrossRef](#)]
33. Pardeshi, S.K.; Pawar, R.Y. SrFe<sub>2</sub>O<sub>4</sub> complex oxide an effective and environmentally benign catalyst for selective oxidation of styrene. *J. Mol. Catal. A Chem.* **2011**, *334*, 35–43. [[CrossRef](#)]
34. Ma, N.; Yue, Y.; Hua, W.; Gao, Z. Selective oxidation of styrene over nanosized spinel-type Mg<sub>x</sub>Fe<sub>3-x</sub>O<sub>4</sub> complex oxide catalysts. *Appl. Catal. A Gen.* **2003**, *251*, 39–47. [[CrossRef](#)]

35. Zhang, Y.; Shen, Z.; Tang, J.; Zhang, Y.; Kong, L.; Zhang, Y. Direct, efficient, and inexpensive formation of  $\alpha$ -hydroxyketones from olefins by hydrogen peroxide oxidation catalyzed by the 12-tungstophosphoric acid/cetylpyridinium chloride system. *Org. Biomol. Chem.* **2006**, *4*, 1478–1482. [[CrossRef](#)]
36. Farzaneh, F.; Asgharpour, Z. Synthesis of a new Schiff base oxovanadium complex with melamine and 2-hydroxynaphthaldehyde on modified magnetic nanoparticles as catalyst for allyl alcohols and olefins epoxidation. *Appl. Organomet. Chem.* **2019**, *33*, e489. [[CrossRef](#)]
37. Silva, N.U.; Fernandes, C.I.; Nunes, T.G.; Saraiva, M.S.; Nunes, C.D.; Vaz, P.D. Performance evaluation of mesoporous host materials in olefin epoxidation using Mo(II) and Mo(VI) active species—Inorganic vs. hybrid matrix. *Appl. Catal. A Gen.* **2011**, *408*, 105–116. [[CrossRef](#)]
38. Al-Ajlouni, A.; Valente, A.A.; Nunes, C.D.; Pillinger, M.; Santos, A.M.; Zhao, J.; Romão, C.C.; Gonçalves, I.S.; Kühn, F.E. Kinetics of Cyclooctene Epoxidation with *tert*-Butyl Hydroperoxide in the Presence of [MoO<sub>2</sub>X<sub>2</sub>L]-Type Catalysts (L = Bidentate Lewis Base). *Eur. J. Inorg. Chem.* **2005**, *9*, 1716–1723. [[CrossRef](#)]
39. Rayati, S.; Moradi, D.; Nejabat, F. Magnetically recoverable porphyrin-based nanocatalysts for the effective oxidation of olefins with hydrogen peroxide: A comparative study. *New J. Chem.* **2020**, *44*, 19385–19392. [[CrossRef](#)]
40. Mortazavi-Manesh, A.; Bagherzadeh, M. Synthesis and characterization of molybdenum (VI) complex immobilized on polymeric Schiff base-coated magnetic nanoparticles as an efficient and retrievable nanocatalyst in olefin epoxidation reactions. *Appl. Organomet. Chem.* **2020**, *34*, e5410. [[CrossRef](#)]
41. Niakan, M.; Asadi, Z.; Masteri-Farahani, M. Immobilization of salen molybdenum complex on dendrimer functionalized magnetic nanoparticles and its catalytic activity for the epoxidation of olefins. *Appl. Surf. Sci.* **2019**, *481*, 394–403. [[CrossRef](#)]
42. Fakhimi, P.; Bezaatpour, A.; Amiri, M.; Szunerits, S.; Boukherroub, R.; Eskandari, H. Manganese Ferrite Nanoparticles Modified by Mo(VI) Complex: Highly Efficient Catalyst for Sulfides and Olefins Oxidation Under Solvent-less Condition. *ChemistrySelect* **2019**, *4*, 7116–7122. [[CrossRef](#)]
43. Gimenez, G.; Nunes, C.D.; Vaz, P.D.; Valente, A.A.; Ferreira, P.; Calhorda, M.J. Hepta-coordinate halocarbonyl molybdenum(II) and tungsten(II) complexes as heterogeneous polymerization catalysts. *J. Mol. Catal. A Chem.* **2006**, *256*, 90–98. [[CrossRef](#)]